Lattice thermal conductivity of disordered NiPd and NiPt alloys

2006 J. Phys.: Condens. Matter 18 4589

(http://iopscience.iop.org/0953-8984/18/19/013)

INSTITUTE OF PHYSICS PUBLISHING JOURNAL OF PHYSICS: CONDENSED MATTER

J. Phys.: Condens. Matter **18** (2006) 4589–4608 doi:10.1088/0953-8984/18/19/013

Lattice thermal conductivity of disordered NiPd and NiPt alloys

Aftab Alam and Abhijit Mookerjee

S N Bose National Centre for Basic Sciences, JD Block, Sector III, Salt Lake City, Kolkata 700098, India

E-mail: alam@bose.res.in and abhijit@bose.res.in

Received 3 January 2006, in final form 3 April 2006
Published 26 April 2006
Online at stacks.iop.org/JPhysCM/18/4589

Abstract

Numerical calculations of lattice thermal conductivity are reported for the binary alloys NiPd and NiPt. The present work is a continuation of an earlier paper by us (Alam and Mookerjee 2005 *Phys. Rev.* B **72** 214207), which developed a theoretical framework for the calculation of configuration-averaged lattice thermal conductivity and thermal diffusivity in disordered alloys. The formulation was based on the augmented space theorem (Mookerjee 1973 *J. Phys. C: Solid State Phys.* **6** L205) combined with a scattering diagram technique. In this paper we shall show the dependence of the lattice thermal conductivity on a series of variables like phonon frequency, temperature and alloy composition. The temperature dependence of $\kappa(T)$ and its relation to the measured thermal conductivity is discussed. The concentration dependence of κ appears to justify the notion of a minimum thermal conductivity as discussed by Kittel, Slack and others (Kittel 1948 *Phys. Rev.* **75** 972, Brich and Clark 1940 *Am. J. Sci.* **238** 613; Slack 1979 *Solid State Physics* vol 34, ed H Ehrenreich, F Seitz and D Turnbull (New York: Academic) p 1). We also study the frequency and composition dependence of the thermal diffusivity averaged over modes. A numerical estimate of this quantity gives an idea about the location of the mobility edge and the fraction of states in the frequency spectrum which is delocalized.

(Some figures in this article are in colour only in the electronic version)

1. Introduction

Lattice thermal conductivity of substitutionally disordered alloys yields valuable information about the interactions of thermal excitations with composition fluctuations on their crystal lattice. Over the past few years numerous experimental studies [4–7] of the thermal conductivity of disordered alloys have provided considerable insight into the nature of their elementary excitations.

The theory of lattice thermal conductivity for perfect crystals and ordered alloys has been set up on a rigorous basis. However, the same is not true for disordered alloys. The presence of disorder results in scattering that not only depends on the impurity concentration but also crucially on both the relative masses and size difference between the constituent atoms. For large mass or size differences, the effect of disorder can be quite unusual. Because of this, detailed comparison between theory and experiment on the basis of realistic models has not been very extensive. Model calculations are mostly based on mean-field approaches with diagonal disorder alone. Whereas in phonon problems essential off-diagonal disorder in the force constants cannot be dealt with within single site mean field approximations. Such disorder effects cannot be ignored in realistic calculations.

When we come to comparison with experiment, however, we face a different kind of difficulty. In any experiment, the measured thermal conductivity κ consists of the sum of an electronic component κ_e and a lattice component κ_L and $\kappa = \kappa_e + \kappa_L$. Assuming the thermal analogue of Matthiessen's rule to be valid, the electronic thermal resistivity $W_e = 1/\kappa_e$ is given by the sum of an ideal resistivity and an impurity or residual term. It is often assumed that the ideal resistivity remains unaltered by alloying and can be obtained from the measurements on pure metals. The residual resistivity W_r can be calculated with the help of the Wiedemann–Franz law $W_r = \rho_0(T)/(L_0T)$, where L_0 is the Lorenz number and $\rho_0(T)$ is determined by measuring the electrical resistivity of the alloy at several temperatures. The lattice component κ_L can then be separated out from the observed conductivity κ. Overall what we would like to convey from these details is that a direct measurement of the lattice component of the thermal conductivity is not feasible. There always exists certain assumptions behind the calculation of κ_e and hence it is not always possible to obtain reliable estimates for this quantity, which consequently affects the separation of κ_L from the observed conductivity κ.

In an earlier communication [1] (hereafter referred to as AM) we had developed a formalism for the calculation of configuration averaged lattice thermal conductivity and thermal diffusivity for a disordered binary alloy. Unlike single-site mean-field approaches, this formulation has no restrictions on what kind of substitutional disorder can be studied. It explicitly takes into account fluctuations in masses, force constants and heat currents. It also maintains, on average, the sum rule between the diagonal and off-diagonal parts of the dynamical matrix which eliminates the translational mode. We had shown that the dominant effect of disorder is to renormalize each propagator as well as the current terms in the Kubo formula.

The purpose of this article is to implement the formulation (AM) for a detailed numerical study of the configuration averaged lattice conductivity and thermal diffusivity for disordered NiPt and NiPd alloys. The choice of the alloy systems is not arbitrary. We have chosen these alloys in order to propose a systematic study of the effects of mass disorder and strong force constant disorder. In the NiPd alloys, mass disorder is much larger than the force constant disorder. However, both kinds of disorder dominate in the NiPt alloys. Moreover, in both the two alloy systems there is a large size mismatch between the constituents. This indicates that the standard single site mean field theories would be inadequate to capture these effects. These alloy systems are therefore ideal for the illustration of the advantages of the augmented space block recursion method proposed by us [8]. Theoretically, there have been many attempts [9–12] to develop an adequate approximation for understanding the lattice thermal conductivity of metals and alloys. The majority were based on model calculations either for perfect crystals or ordered alloys. One of the most successful mean-field approximations was the coherent potential approximation (CPA) [13] in combination with the appropriate Kubo formula. The CPA is a single site mean-field theory capable of dealing only with mass disorder. There have been many attempts to generalize the CPA in order to treat both off-diagonal and

environmental disorder. In many cases these approximations did not satisfy the necessary Herglotz–Sokhotsky–Plemelj (HSP) analytic and lattice translational invariance properties of the configuration averaged Green functions. Two very similar approaches, both based on the augmented space theorem, have been recently proposed: the itinerant cluster CPA (ICPA) [14] and the augmented space recursion [15]. These have been used to study the lattice dynamics of $Ni_{55}Pd_{45}$, $Ni_{50}Pt_{50}$ and $Ni_{88}Cr_{12}$ alloys. In a more generalized context of inelastic neutron scattering in disordered alloys, an augmented space block recursion (ASBR) has also been proposed recently [8]. The ASBR calculates the full Green and self-energy matrices instead of their diagonal entries alone. These are required for obtaining the response functions.

In this paper, we shall make use of the ASBR technique to implement the theoretical formulation for the lattice thermal conductivity developed earlier by us. We shall study the dependence of lattice thermal conductivity on phonon frequency as well as on temperature in a series of disordered NiPd and NiPt alloys covering the full range of alloy compositions.

As far as the temperature dependence of lattice conductivity is concerned, our results follow a general trend. We shall also discuss how the lattice conductivity behaves as a function of concentration at several fixed temperatures. The notion of a minimum thermal conductivity will be justified. It will be shown that low temperature resonant modes considerably decrease the conductivity. An idea about the location of the mobility edge will be discussed from the phonon-frequency dependence of the mode averaged harmonic diffusivity. This dependence also gives a rough idea about what fraction of the states across the frequency spectrum are delocalized and therefore can carry current. The concentration dependence of the harmonic diffusivity will also be displayed.

2. Theoretical formulation

In the next two subsections, we shall apply the formalism introduced in our earlier paper (AM) to study NiPd and NiPt alloys across the alloy composition range. In AM we have discussed the theoretical formalism in great detail. We shall present only the main points here and leave the reader to refer to AM for greater detail.

The derivation of a Kubo formula for thermal conductivity requires an additional statistical hypothesis, which states that a system in steady state has a space dependent *local* temperature $T(\mathbf{r}_i) = [\kappa_B \beta(\mathbf{r}_i)]^{-1}$. The matrix element of the heat current in the basis of the eigenfunctions of the Hamiltonian is given by:

$$\mathbf{S}^{\mu}_{\gamma\gamma'}(\mathbf{k}) = \frac{h}{2}\left(\nu_{\mathbf{k}\gamma} + \nu_{\mathbf{k}\gamma'}\right)\mathbf{v}^{\mu}_{\gamma\gamma'}(\mathbf{k}),$$

where the phonon group velocity $\mathbf{v}_{\gamma\gamma'}(\mathbf{k})$ is given by

$$\mathbf{v}_{\gamma\gamma'} = \frac{1}{2\sqrt{\nu_{\mathbf{k}\gamma}\,\nu_{\mathbf{k}\gamma'}}}\sum_{\mu}\sum_{\nu}\epsilon^{\mu}_{\gamma}(\mathbf{k})\nabla_{\mathbf{k}}D^{\mu\nu}(\mathbf{k})\epsilon^{\nu}_{\gamma'}(\mathbf{k});$$

here γ, γ' label the various modes of vibration, $\nu_{\mathbf{k}\gamma}$, $\nu_{\mathbf{k}\gamma'}$ are their frequencies, $\epsilon^{\mu}_{\gamma}(\mathbf{k})$, $\epsilon^{\nu}_{\gamma'}(\mathbf{k})$ are the polarization vectors and $D^{\mu\nu}(\mathbf{k})$ is the Fourier transform of the mass scaled dynamical matrix.

We shall consider the case where the temperature gradient is uniform within the system. The linear response formula then relates the linear heat current response to the temperature gradient field

$$\langle S^{\mu}(t)\rangle = -\sum_{\nu}\int_{-\infty}^{\infty} \mathrm{d}t'\kappa^{\mu\nu}(t-t')\nabla^{\nu}\delta T(t),$$

where the generalized susceptibility $\kappa^{\mu\nu}(t-t')$ is given by the Kubo formula,

$$\kappa^{\mu\nu}(\tau) = \Theta(\tau)\frac{1}{T}\int_0^\beta \mathrm{d}\lambda \langle S^\mu(-\mathrm{i}\hbar\lambda), S^\nu(\tau)\rangle,$$

$\Theta(\tau)$ is the Heaviside step function, and

$$S(-\mathrm{i}\hbar\lambda) = \mathrm{e}^{\lambda H} S \mathrm{e}^{-\lambda H}.$$

$\langle\ \rangle$ on the right-hand side of the above equation denotes thermal averaging over states in the absence of a temperature gradient. The above equation can be rewritten in the form of a Kubo–Greenwood expression

$$\begin{aligned}
\kappa^{\mu\nu}(\nu, T) &= \kappa_{\mathrm{I}}^{\mu\nu}(\nu, T) + \kappa_{\mathrm{II}}^{\mu\nu}(\nu, T) \\
\kappa_{\mathrm{I}}^{\mu\nu}(\nu, T) &= \frac{\pi}{T}\int \frac{\mathrm{d}^3\mathbf{k}}{8\pi^3}\sum_\gamma \sum_{\gamma'\neq\gamma} \frac{\langle n_{\mathbf{k}\gamma'}\rangle - \langle n_{\mathbf{k}\gamma}\rangle}{h(\nu_{\mathbf{k}\gamma} - \nu_{\mathbf{k}\gamma'})} \mathbf{S}^\mu_{\gamma\gamma'}(\mathbf{k})\mathbf{S}^\nu_{\gamma'\gamma}(\mathbf{k})\delta(\nu_{\mathbf{k}\gamma} - \nu_{\mathbf{k}\gamma'} - \nu) \qquad (1) \\
\kappa_{\mathrm{II}}^{\mu\nu}(\nu, T) &= \frac{1}{\kappa_{\mathrm{B}}T^2}\left[\left\{\int \frac{\mathrm{d}^3\mathbf{k}}{8\pi^3}\sum_\gamma \langle n_{\mathbf{k}\gamma}\rangle \mathbf{S}^\mu_{\gamma\gamma}(\mathbf{k})\right\}\left\{\int \frac{\mathrm{d}^3\mathbf{k}}{8\pi^3}\sum_\gamma \langle n_{\mathbf{k}\gamma}\rangle \mathbf{S}^\nu_{\gamma\gamma}(\mathbf{k})\right\}\right. \\
&\quad \left. - \kappa_{\mathrm{B}}T\int \frac{\mathrm{d}^3\mathbf{k}}{8\pi^3}\sum_\gamma \frac{\partial\langle n_{\mathbf{k}\gamma}\rangle}{\partial(h\nu_{\mathbf{k}\gamma})} S^\mu_{\gamma\gamma}(\mathbf{k})S^\nu_{\gamma\gamma}(\mathbf{k})\right]\delta(\nu) \qquad (2)
\end{aligned}$$

where $\langle n_{\mathbf{k}\gamma}\rangle = (\mathrm{e}^{\beta h\nu_{\mathbf{k}\gamma}} - 1)^{-1}$ is the equilibrium Bose–Einstein distribution function and T is the absolute temperature.

The first expression is for inter-band transitions, while the second expression is for intra-band transitions. For an isotropic response, we can rewrite the first expression as

$$\kappa_{\mathrm{I}}(\nu, T) = \frac{\pi}{3T}\sum_\mu \int \mathrm{d}\nu' \int \frac{\mathrm{d}^3\mathbf{k}}{8\pi^3}\sum_{\gamma\gamma'} \hat{\mathbf{S}}^\mu_{\gamma\gamma'}(\mathbf{k}, T)\hat{\mathbf{S}}^\mu_{\gamma'\gamma}(\mathbf{k}, T)\delta(\nu' - \nu_{\mathbf{k}\gamma'})\delta(\nu' + \nu - \nu_{\mathbf{k}\gamma})$$

where

$$\hat{\mathbf{S}}^\mu_{\gamma\gamma'}(\mathbf{k}, T) = \sqrt{\left|\frac{\langle n_{\mathbf{k}\gamma'}\rangle - \langle n_{\mathbf{k}\gamma}\rangle}{h(\nu_{\mathbf{k}\gamma} - \nu_{\mathbf{k}\gamma'})}\right|}\mathbf{S}^\mu_{\gamma\gamma'}(\mathbf{k}).$$

We may rewrite the above equation as

$$\begin{aligned}
\kappa_{\mathrm{I}}(\nu, T) = \frac{1}{3\pi T}\sum_\mu \int \mathrm{d}\nu' \int \frac{\mathrm{d}^3\mathbf{k}}{8\pi^3}&\mathrm{Tr} \\
&\times \left[\hat{\mathbf{S}}^\mu(\mathbf{k}, T)\mathrm{Im}\{\mathbf{G}(\mathbf{k}, \nu')\}\hat{\mathbf{S}}^\mu(\mathbf{k}, T)\mathrm{Im}\, m\{\mathbf{G}(\mathbf{k}, \nu' + \nu)\}\right].
\end{aligned}$$

The operator $\mathbf{G}(\nu)$ is the phonon Green operator $(M\nu^2\mathbf{I} - \mathbf{\Phi})^{-1}$. The trace is invariant in different representations. For crystalline systems, usually the Bloch basis $\{|\mathbf{k}, \gamma\rangle\}$ is used. For disordered systems, prior to configuration averaging, it is more convenient to use the basis $\{|\mathbf{k}, \alpha\rangle\}$, where $\mathbf{k}$ is the reciprocal vector and α represents the coordinate axis directions. We can transform from the mode basis to the coordinate basis by using the transformation matrices $\Upsilon_{\gamma\alpha}(\mathbf{k}) = \epsilon^\alpha_\gamma(\mathbf{k})$. For example,

$$\hat{\mathbf{S}}^\mu_{\alpha\beta}(\mathbf{k}, T) = \Upsilon^{-\mathrm{T}}_{\alpha\gamma}(\mathbf{k})\hat{\mathbf{S}}^\mu_{\gamma\gamma'}(\mathbf{k}, T)\Upsilon^{-1}_{\gamma'\beta}(\mathbf{k}).$$

If we define

$$\boldsymbol{\kappa}(z_1, z_2) = \int \frac{\mathrm{d}^3\mathbf{k}}{8\pi^3}\mathrm{Tr}\left[\hat{\mathbf{S}}\mathbf{G}(\mathbf{k}, z_1)\hat{\mathbf{S}}\mathbf{G}(\mathbf{k}, z_2)\right] \qquad (3)$$

then the above equation becomes

$$\kappa(\nu, T) = \frac{1}{12\pi T}\sum_{\mu}\int \mathrm{d}\nu'[\boldsymbol{\kappa}^{\mu\mu}(\nu'^{-}, \nu'^{+} + \nu) + \boldsymbol{\kappa}^{\mu\mu}(\nu'^{+}, \nu'^{-} + \nu) - \boldsymbol{\kappa}^{\mu\mu}(\nu'^{+}, \nu'^{+} + \nu) - \boldsymbol{\kappa}^{\mu\mu}(\nu'^{-}, \nu'^{-} + \nu)] \tag{4}$$

where

$$f(\nu^{+}) = \lim_{\delta\to 0} f(\nu + \mathrm{i}\delta), \qquad f(\nu^{-}) = \lim_{\delta\to 0} f(\nu - \mathrm{i}\delta).$$

We have used the HSP analytic property [15] of the Green operator

$$\mathbf{G}(\nu + \mathrm{i}\delta) = \mathrm{Re}\,[\mathbf{G}(\nu)] - \mathrm{i}\,\mathrm{sgn}\,(\delta)\mathrm{Im}\,[\mathbf{G}(\nu)]\,.$$

For disordered materials, we shall be interested in obtaining the configuration averaged response functions. This will require the configuration averaging of quantities like $\kappa(z_1, z_2)$. This averaging procedure we have discussed in detail in AM:

$$\langle\langle\kappa(z_1, z_2)\rangle\rangle = \langle\langle\kappa_{(1)}(z_1, z_2)\rangle\rangle + \langle\langle\Delta\kappa(z_1, z_2)^{\mathrm{ladder}}\rangle\rangle. \tag{5}$$

The first term in the right hand side stands for the disorder induced corrections where the disorder scattering renormalizes the phonon propagators as well as the heat currents. In this term, corrections to the heat current are related to the self-energy of the propagators. The second term of equation (5) includes the vertex corrections due to the correlated propagation.

For a harmonic solid, a temperature independent mode diffusivity D_γ is defined as

$$D_{\gamma}^{\mu\nu}(\mathbf{k}) = \pi\sum_{\gamma'\neq\gamma}\frac{1}{\nu_{\mathbf{k}\gamma}^{2}}\mathbf{S}_{\gamma\gamma'}^{\mu}(\mathbf{k})\mathbf{S}_{\gamma'\gamma}^{\nu}(\mathbf{k})\delta(\nu_{\mathbf{k}\gamma} - \nu_{\mathbf{k}\gamma'}).$$

The independent mode diffusivity is an intrinsic property of the γth normal mode and provides an unambiguous criterion for localization.

The averaged thermal diffusivity (averaged over modes) is then given by

$$\mathbf{D}^{\mu\nu}(\nu) = \frac{\int\frac{\mathrm{d}^3\mathbf{k}}{8\pi^3}\sum_{\gamma}D_{\gamma}^{\mu\nu}(\mathbf{k})\delta(\nu - \nu_{\mathbf{k}\gamma})}{\int\frac{\mathrm{d}^3\mathbf{k}}{8\pi^3}\sum_{\gamma}\delta(\nu - \nu_{\mathbf{k}\gamma})} = \frac{D_{\mathrm{tot}}^{\mu\nu}(\nu)}{\int\frac{\mathrm{d}^3\mathbf{k}}{8\pi^3}\sum_{\gamma}\delta(\nu - \nu_{\mathbf{k}\gamma})}.$$

Assuming isotropy of the response, we can rewrite the numerator of the above equation as

$$D_{\mathrm{tot}}^{\mu\mu}(\nu) = \pi\int\mathrm{d}\nu'\int\frac{\mathrm{d}^3\mathbf{k}}{8\pi^3}\sum_{\gamma}\sum_{\gamma'}\hat{S}_{\gamma\gamma'}^{\mu}(\mathbf{k})\hat{S}_{\gamma'\gamma}^{\mu}(\mathbf{k})\delta(\nu' - \nu_{\mathbf{k}\gamma'})\delta(\nu_{\mathbf{k}\gamma} - \nu')\delta(\nu - \nu_{\mathbf{k}\gamma})$$

where

$$\hat{S}_{\gamma\gamma'}^{\mu}(\mathbf{k}) = \frac{1}{\nu_{\mathbf{k}\gamma}}\mathbf{S}_{\gamma\gamma'}^{\mu}(\mathbf{k}).$$

We may again rewrite the above equation for D_{tot} as

$$D_{\mathrm{tot}}^{\mu\mu}(\nu) = \frac{1}{\pi^2}\int\mathrm{d}\nu'\int\frac{\mathrm{d}^3\mathbf{k}}{8\pi^3}\mathrm{Tr}\left[\mathrm{Im}\,\{\mathbf{G}(\mathbf{k}, \nu')\}\hat{\mathbf{S}}^{\mu}(\mathbf{k})\mathrm{Im}\,m\{\mathbf{G}(\mathbf{k}, \nu')\}\hat{\mathbf{S}}^{\mu}(\mathbf{k})\mathrm{Im}\,m\{\mathbf{G}(\mathbf{k}, \nu)\}\right].$$

The averaged thermal diffusivity can then be expressed as (for an isotropic response)

$$\mathbf{D}(\nu) = \frac{1}{3}\sum_{\mu}D^{\mu\mu}(\nu) = \frac{\pi}{3}\frac{\sum_{\mu}\mathbf{D}_{\mathrm{tot}}^{\mu\mu}(\nu)}{\int\frac{\mathrm{d}^3\mathbf{k}}{8\pi^3}\mathrm{Tr}\,[\mathrm{Im}\,\{\mathbf{G}(\mathbf{k}, \nu)\}]}. \tag{6}$$

For disordered material, we shall be interested as before in obtaining the configuration averaged thermal diffusivity. The configuration averaged thermal diffusivity can be expressed (to a first order approximation) in the form

$$\langle\langle\mathbf{D}(\nu)\rangle\rangle = \frac{\pi}{3}\frac{\sum_{\mu}\langle\langle\mathbf{D}_{\mathrm{tot}}^{\mu\mu}(\nu)\rangle\rangle}{\int\frac{\mathrm{d}^3\mathbf{k}}{8\pi^3}\mathrm{Tr}\,[\mathrm{Im}\,\langle\langle\mathbf{G}(\mathbf{k}, \nu)\rangle\rangle]}, \tag{7}$$

where

$$\langle\langle D_{\rm tot}^{\mu\mu}(\nu)\rangle\rangle \simeq \frac{1}{\pi^2}\int {\rm d}\nu' \int \frac{{\rm d}^3\mathbf{k}}{8\pi^3}{\rm Tr}\left[{\rm Im}\,\langle\langle \mathbf{G}(\mathbf{k},\nu')\rangle\rangle \right.$$
$$\left. \langle\langle \hat{\mathbf{S}}^{\mu}(\mathbf{k}){\rm Im}\,\{\mathbf{G}(\mathbf{k},\nu')\}\hat{\mathbf{S}}^{\mu}(\mathbf{k}){\rm Im}\,\{\mathbf{G}(\mathbf{k},\nu)\}\rangle\rangle\right].$$

3. Results and discussion

The details of numerical calculation for the two alloys of our interest in the present work are as follows.

- We have carried out calculations on 501 ν-points.
- A small imaginary part of the frequency $\delta = 0.001$ has been used for evaluating the Green matrix and self-energy matrix in the augmented space block recursion [8].
- The calculation of lattice conductivity has been done at 40 temperatures.
- For the Brillouin zone integration, 145 $\mathbf{k}$-points in the irreducible 1/48th of the zone produced well converged results.

3.1. NiPd alloy: strong mass and weak force constant disorder

For a list of general properties of fcc Ni and Pd, we refer the reader to [15]. This particular alloy has already been studied experimentally by Farrell and Greig [4] using conventional potentiometric techniques. But unfortunately their investigation was limited only to very dilute alloys in the temperature range 2–100 K. In an earlier communication (AM) we have already shown a comparison of our results for the temperature dependence of thermal conductivity with theirs for a dilute $Ni_{99}Pd_{01}$ alloy.

Our initial focus in the earlier communication [1] was to calculate the effect of disorder scattering over an averaged medium. We had made use of the multiple scattering diagram technique and went beyond the framework of CPA, which treats only diagonal disorder. Rather we had applied the technique in a more generalized context with the inclusion of diagonal as well as off-diagonal disorder arising out of the disorder in the dynamical matrix. In an attempt to compare the effect of averaged heat current and disorder induced renormalized heat current on the lattice thermal conductivity, we have plotted figure 1.

Figure 1 shows the results for disordered $Ni_{50}Pd_{50}$ alloy. The heavy curve represents the lattice conductivity including all kinds of disorder induced corrections, e.g. corrections to the heat current and the vertex corrections, while the medium curve stands for the same quantity but using averaged heat currents and without vertex corrections. The grey curve indicates the configuration averaged joint density of states. From the figure it is clear that $\tau = |S_{\rm eff}(\nu, T)|^2$ is strongly dependent both on the initial and the final energies throughout the phonon frequency (ν). That is,

$$\kappa(\nu, T) \neq \tau(\nu, T)J(\nu), \tag{8}$$

where $J(\nu)$ is the joint density of states given by

$$J(\nu) = \int {\rm d}\nu' \int \frac{{\rm d}^3\mathbf{k}}{8\pi^3}{\rm Tr}\left[{\rm Im}\,\langle\langle \mathbf{G}(\mathbf{k},\nu')\rangle\rangle {\rm Im}\,\langle\langle \mathbf{G}(\mathbf{k},\nu'+\nu)\rangle\rangle\right]. \tag{9}$$

Figure 1 shows that the effect of disorder corrections to the current terms on the overall shape of lattice conductivity is rather small in the $Ni_{50}Pd_{50}$ alloy. We should note that the effect of disorder corrections to current and the vertex corrections in these alloys becomes negligible beyond phonon frequencies $\simeq$2.5 THz. For the higher frequency modes the effect of the scattering phenomenon is well described by the mean-field approximation. It is in

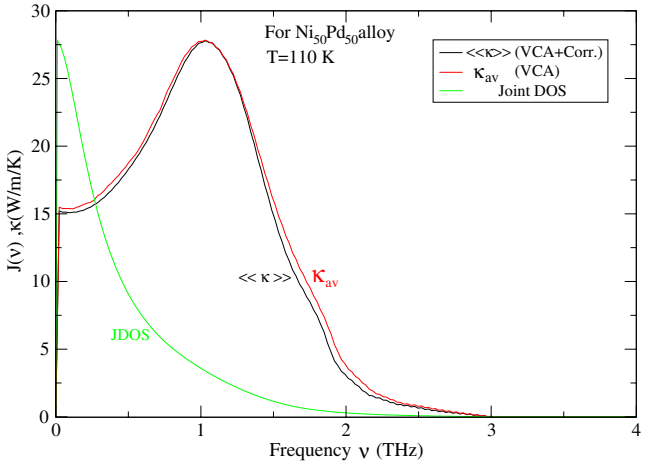

Figure 1. Configuration averaged lattice thermal conductivity versus phonon frequency ν (THz) for $Ni_{50}Pd_{50}$ disordered alloy. The medium and heavy black lines show the conductivity using the average VCA current and effective current (consisting of average VCA current + disorder corrections + vertex correction) respectively. The grey line indicates the configuration averaged joint density of states.

the low frequency region that configuration fluctuation effects beyond the mean field become significant.

There is a very important feature in figure 1 that still needs discussion, which is how to explain the origin of a dip in $\kappa(\nu)$ at the lowest energy $\nu = 0$. A similar kind of dip has also been reported by Feldman *et al* [16] while studying amorphous Si and $Si_{1-x}Ge_x$ alloys. Their $\kappa(\nu)$ have a small Lorentzian shaped dip at $\nu = 0$. This reflects the missing intraband conductivity κ^{II}. This dip in $\kappa(\nu)$ stands at a small but finite value ($\nu \simeq 0$). The finiteness of the dip in $\kappa(\nu)$ is because of the fact that their calculation was based on a Kubo–Greenwood expression for the thermal conductivity with the delta functions in the expression broadened into a Lorentzian of small (but finite) width η. However, in our case it is evident from figure 1 that this dip in $\kappa(\nu)$ stands at $\kappa(\nu) \to 0$ at $\nu = 0$. This is due to the simple fact that in our calculation the Lorenzian broadening has not been put in by hand, but it arises automatically from the disorder effect on the crystalline spectral function $\mathrm{Im}\, m[\mathbf{G}(\mathbf{k}, \nu)]$. Another reason for this difference in the position of the dip in $\kappa(\nu)$ may be due to the fact that Feldman *et al* carried out their calculation at a fixed wavevector $\mathbf{k}$, while we have summed over the entire Brillouin zone.

The origin of this dip can also be explained by looking at the joint density of states (JDOS) represented by a grey line in figure 1. This quantity has a dip near $\nu = 0$ reminiscent of the dip in the $\kappa(\nu)$ curves. This indicates that a smooth convolution of two Green matrices $\mathbf{G}(\mathbf{k}, \nu')$ and $\mathbf{G}(\mathbf{k}, \nu' + \nu)$ (or two smooth densities of states obtained after summing $\mathbf{k}$ over the Brillouin zone), as appeared in the expression (5) of [1], is mainly responsible for such a sharp dip in the lattice conductivity at $\nu = 0$. As discussed by Feldman *et al*, this dip at $\nu = 0$ disappears as the system size $N \to \infty$. They have also suggested an appropriate method to eliminate this dip in a sensible manner, which allows us to extrapolate the $\kappa(\nu)$ curve from a value at $\nu > 0$ ($\nu \simeq 0$) to a value at $\nu = 0$. This extrapolated value of $\kappa(\nu)$ at $\nu = 0$ is nothing but the dc value of the lattice thermal conductivity κ_0. In an attempt to calculate (κ_0), we have obtained a value of 15.25 W m^{-1} K^{-1} for $Ni_{50}Pd_{50}$ alloy at $T = 110$ K.

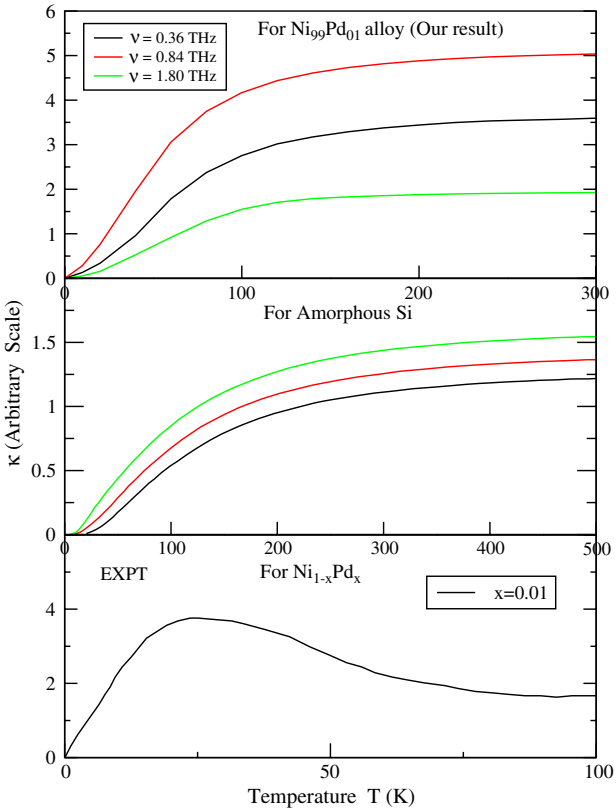

Figure 2. Thermal conductivity versus temperature T(K) for NiPd alloys and amorphous Si. The top panel shows our results on the lattice conductivity for $Ni_{99}Pd_{01}$ alloy at three different frequency cut-offs ν. The middle panel shows the lattice conductivity for amorphous Si [16] at three different cut-off frequencies, while the panel at the bottom shows the experimental data [4] for the total thermal conductivity (= lattice + electronic contribution) of the same $Ni_{99}Pd_{01}$ alloy.

Direct comparison with the experimental data on these systems is difficult, because the experimental thermal conductivity also has a component arising out of the contribution from electrons. Figure 2 shows the temperature dependence of lattice conductivity. The top panel shows our theoretical result for the $Ni_{99}Pd_{01}$ alloy at three different frequencies. The bottom panel shows the experimental data [4] on the total (electronic and lattice) thermal conductivity of the same 99-01 NiPd alloy. Since the frequency is not mentioned in the experimental data, we assume that it must be for low frequencies. The best comparison then will be between the middle (black) curve on the top panel and that in the bottom one. The two agree qualitatively, except at low temperatures, where we expect the electronic contribution to dominate. In order to understand whether the deviation *does arise* from the electronic contribution, we have compared the top panel with the thermal conductivity of amorphous Si [16], shown in the middle panel. In a-Si the electrons near the Fermi level are localized and hence cannot carry any current. The contribution to thermal conductivity arises from scattering due to configuration fluctuations in the amorphous material. Qualitatively, we expect the results to be similar to configuration fluctuation scattering in random alloys. Almost the entire contribution should come from the phonons. The behaviours of the two panels are quite similar. The origin of the hump in the experimental lattice conductivity can also be understood if we assume the

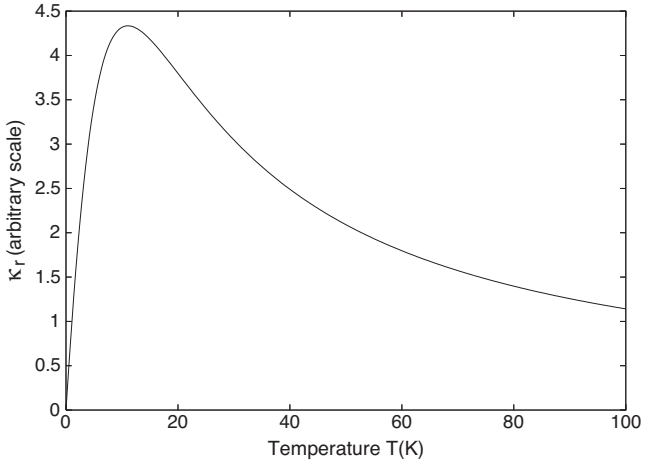

Figure 3. Residual or impurity contribution of the electronic part of the thermal conductivity.

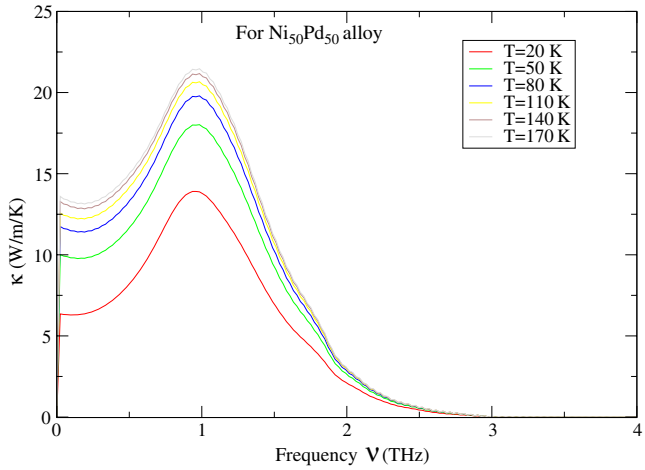

Figure 4. The configuration averaged lattice thermal conductivity versus phonon frequency ν (THz) at different temperatures T for $Ni_{50}Pd_{50}$ alloy.

Wiedemann–Franz law and write the residual part of the electronic contribution of the thermal resistivity as $\kappa_r = L_0 T/\rho_0(T)$. Here L_0 is the Lorenz number and $\rho_0(T)$ is the electrical resistivity. Assuming that the electrical resistivity behaves as $\rho_0(T) = A + BT + CT^2$ at low temperatures and with a suitable choice of the parameters, this contribution does show a hump followed by a decreasing behaviour flattening out at larger temperatures (see figure 3). The sum of the contribution shown in the top panel of figure 2 and that in figure 3 would lead to the experimental behaviour shown in the bottom panel of figure 2. This is a plausibility argument and needs to be confirmed by a detailed calculation of the electronic contribution to the thermal conductivity.

We shall now present the dependence of lattice thermal conductivity and thermal diffusivity on parameters such as phonon frequency (ν), concentration (x) etc. In figure 4, we display the frequency dependence of lattice conductivity for $Ni_{50}Pd_{50}$ alloy at various temperatures

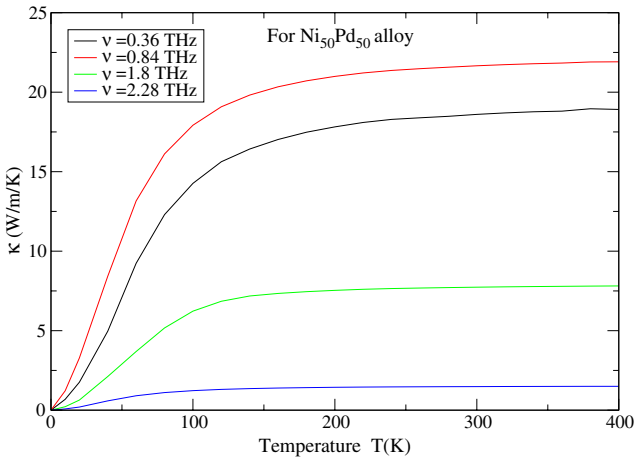

Figure 5. The averaged lattice thermal conductivity versus temperature T (K) at various cut-off frequencies ν_{cutoff} for $Ni_{50}Pd_{50}$ alloy.

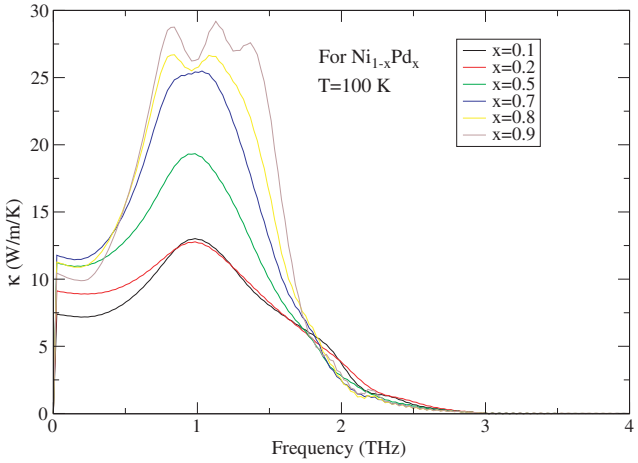

Figure 6. Frequency dependence of lattice thermal conductivity for various alloys $Ni_{1-x}Pd_x$ at $T = 100$ K.

evaluated using equation (5). The figure clearly shows the saturation of lattice conductivity as we proceed towards the higher temperatures. The dc value of the conductivity (κ_0), which is just an extrapolation of the $\kappa(\nu)$ curve from a value at $\nu > 0$ to a value at $\nu = 0$, increases as we increase the temperature.

The temperature dependence of lattice thermal conductivity for the $Ni_{50}Pd_{50}$ alloy at various phonon frequencies ν is shown in figure 5. It is qualitatively similar to $Ni_{50}Pt_{50}$ alloy. The conductivity initially increases with temperature, reflecting a quadratic T-dependence (in the low T regime) and ultimately reaches a T-independent saturated value (at higher temperatures).

Figure 6 shows the lattice conductivity as a function of frequency at $T = 100$ K for various alloy compositions. Comparing the results of figure 6 with those of figure 14 for NiPt,

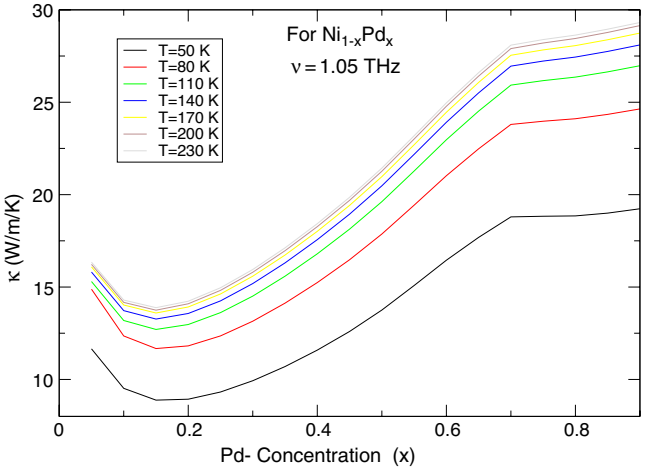

Figure 7. Lattice thermal conductivity versus Pd concentration for various temperatures T at phonon frequency $\nu = 1.05$ THz.

it is clear at a glance that the overall shape of frequency dependence of κ for various alloys of $Ni_{1-x}Pd_x$ looks similar; however, for $x = 0.8$ and $x = 0.9$ extra structure appears in the frequency dependence. Similar behaviour has also been observed for $x = 0.9$ in $Ni_{1-x}Pt_x$ alloy in figure 14. We believe that this behaviour for $Ni_{1-x}Pd_x$ alloy at $x = 0.8$ and 0.9 may be due to the strong disorder in masses, the effect of which becomes important in the two dilute limit alloys. Such an anomalous behaviour is also reflected in the concentration dependence of lattice conductivity. This is shown in figure 7, which plots the lattice conductivity versus Pd concentration (x) at a fixed frequency $\nu = 1.05$ THz for various temperatures.

The thermal diffusivities $D(\nu)$ are important because the effect of disorder is often manifested in them more directly than in the conductivities. Not only that thermal diffusivity also gives an approximate idea about the location of the mobility edge as well as the fraction of delocalized states. In figure 8 we display the thermal diffusivity $D(\nu)$ versus frequency for various compositions. The extent of the phonon frequency spectrum is shown by the broad lines. The density of states is non-zero across this spectrum range. The first thing to note is that the region of large diffusivity in the five sets of alloys at the higher frequency side is not the same. In other words, the weakly defined humps on the lower as well as higher frequency side are located at different positions for different alloys. The low frequency maximum in diffusivity is a minimum around the 50–50 composition where the disorder scattering is the maximum. Above 2.8 THz, there is a smooth decrease of diffusivity approximately linear in frequency $D(\nu) \propto (\nu_c - \nu)^\alpha$, with the critical exponent $\alpha \simeq 1$ and a critical frequency ν_c where $D(\nu)$ vanishes to within a very small level of noise. The allowed phonon states beyond this frequency must be due to localized phonon modes. The critical frequency ν_c locates the mobility edge above which the diffusivity is strictly zero in the infinite size limit. Once the mobility edge is located, the fraction of de-localized states may be estimated directly. It is clear from the figure that the location of the mobility edge varies with composition. Consequently, the percentage of de-localized states available for thermal conduction in the system also varies with composition. An inspection of figure 8 determines the location of the mobility edges (ν_c) for the five different compositions. Figure 9, which shows the position of the mobility edge and the percentage of mobile phonon states in the spectrum as a function of the composition, is quite illustrative.

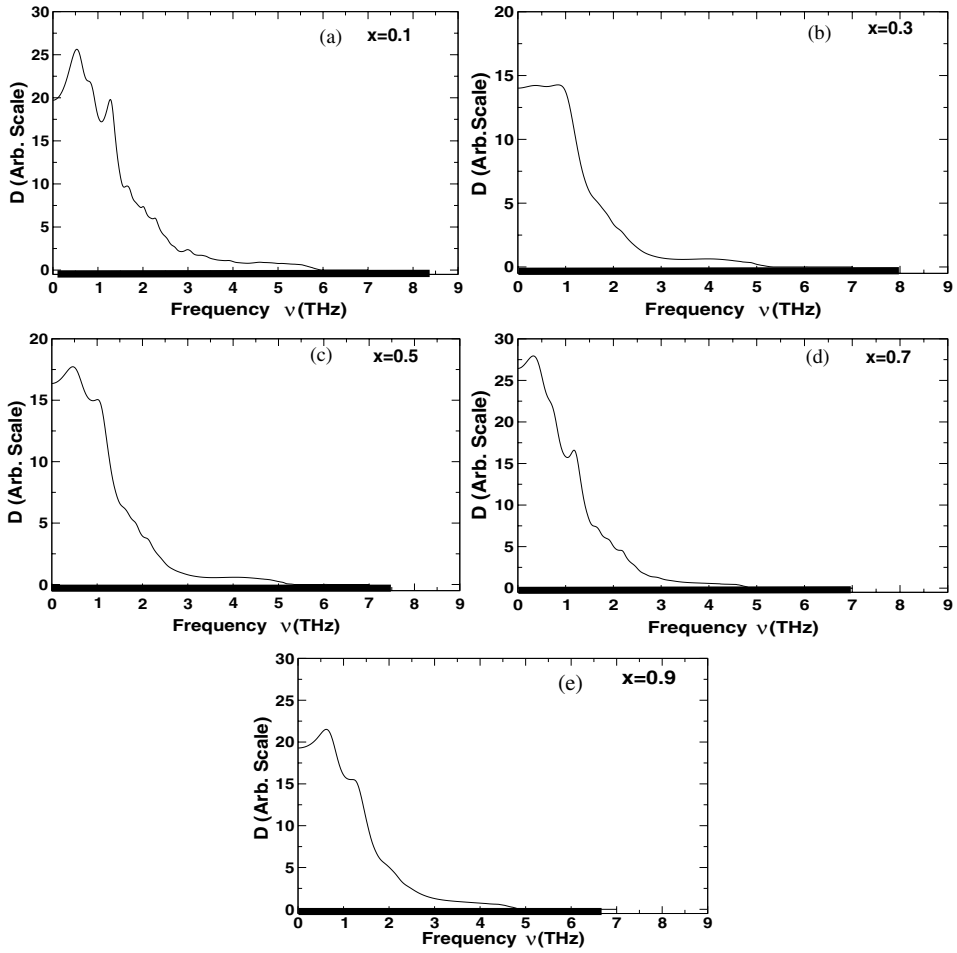

Figure 8. The configuration averaged thermal diffusivities $D(\nu)$ for $Ni_{1-x}Pd_x$ alloys. (a) $x = 0.1$; (b) $x = 0.3$; (c) $x = 0.5$; (d) $x = 0.7$; (e) $x = 0.9$. The broad line on the frequency axis shows the extent of the vibrational spectrum.

The maximum percentage of localized states occurs at 50–50 composition, where we expect disorder scattering to be a maximum. The mobility edge moves to higher frequencies as the concentration of Ni increases, but so does the band width of the phonon spectrum. The minimum percentage of mobile phonon states available for thermal conduction occurs, as expected, at around the 50–50 composition. A similar behaviour has also been discussed by Feldman *et al* [16] while studying the effects of mass disorder on various $Si_{1-x}Ge_x$ alloys.

Figure 10 shows the concentration dependence of thermal diffusivity for $Ni_{1-x}Pd_x$ alloy at various frequencies (ν). As expected from our earlier discussion, the minimum diffusivity occurs around the 50–50 composition, where disorder scattering is maximum. The curves have asymmetry around $x = 0.5$, which decreases with increasing frequency. This asymmetry reflects a similar asymmetry in the thermal conductivity as a function of composition.

3.2. NiPt alloy: strong mass and force constant disorder

We refer the reader to a previous article [15] by us for some of the basic properties of fcc Ni and Pt which is relevant for our present calculation. It has been our experience [15, 8] that

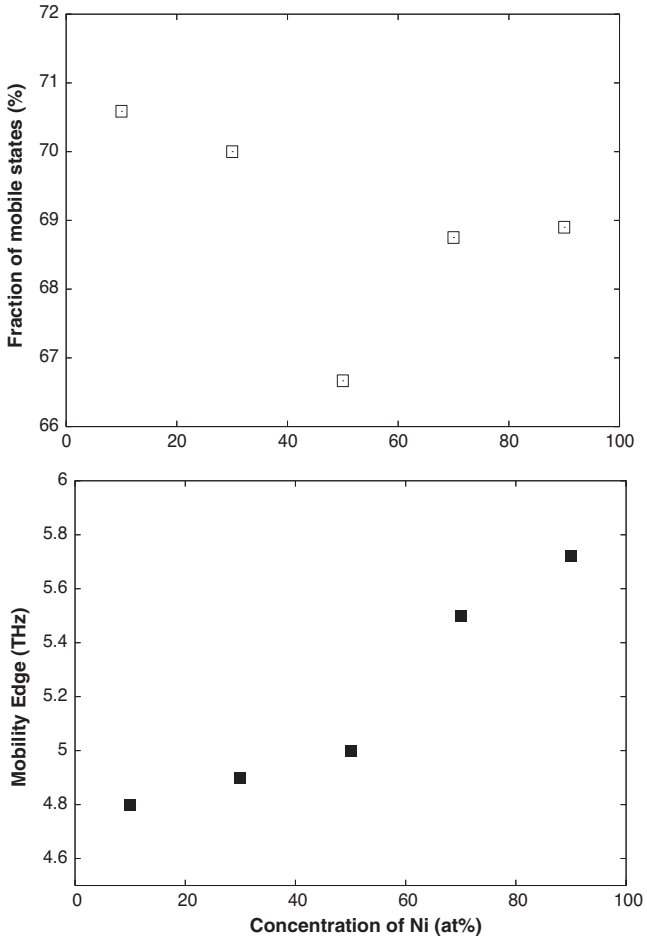

Figure 9. The position of the mobility edge (bottom) and the percentage of mobile phonon states (top) as a function of the alloy composition for NiPd alloy.

the effect of disorder in NiPt alloy is more dramatic than NiPd, for instance the appearance of sharp discontinuities observed in the dispersion where we have resonance states and consequent increase in the line-width [15].

Figure 11 shows the results for disordered $Ni_{50}Pt_{50}$ alloy. As before, the heavy black curve represents the lattice conductivity including all kinds of disorder induced corrections, e.g. corrections to the heat current and the vertex corrections, while the medium curve stands for the same quantity but using averaged heat currents and without vertex corrections. The grey curve shows the scaled joint density of states. From the figure it is clear that as in the case of NiPd the transition rate 'τ' is strongly dependent both on the initial and the final energies throughout the phonon frequency (ν). Figure 11 also clarifies that although the effect of disorder corrections to the current terms is small this effect is comparatively more pronounced in $Ni_{50}Pt_{50}$ than in $Ni_{50}Pd_{50}$. The effect of disorder corrections to current and the vertex corrections in the present case become negligible beyond phonon frequencies $\simeq$2.4 THz. In the low frequency region, configuration fluctuation effects beyond the mean field are more pronounced in NiPt than in NiPd. This may be because of two simple physical factors: first,

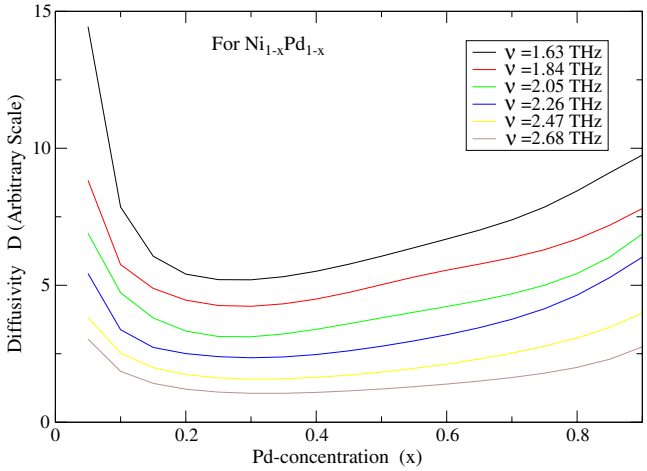

Figure 10. The averaged thermal diffusivity $D(\nu)$ versus Pd concentration at various cut-off frequencies ν_{cutoff} for $Ni_{1-x}Pd_x$ alloy.

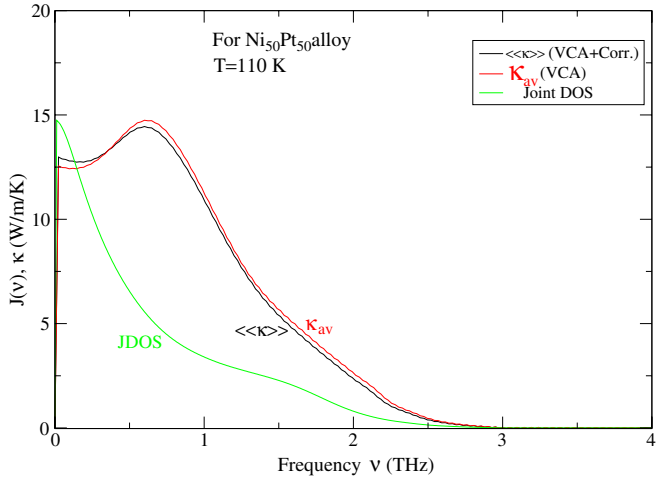

Figure 11. Configuration averaged lattice thermal conductivity versus phonon frequency ν (THz) for $Ni_{50}Pt_{50}$ disordered alloy. The medium and heavy black curves show the conductivity using the average VCA current and effective current (consisting of average VCA current + disorder corrections + vertex correction) respectively. The grey curve indicates the configuration averaged joint density of states.

NiPt is an alloy where both mass ($m_{\text{Pt}}/m_{\text{Ni}} \simeq 3$) as well as force constant (Pt force constants are on average 55% larger than those of Ni) disorder dominates, while in NiPd alloy the mass disorder ($m_{\text{Pd}}/m_{\text{Ni}} \simeq 1.812$) is weaker than NiPt and the force constants are almost the same for the two constituents. Second, from a purely phenomenological point of view, there is a larger size mismatch between Ni and Pt in NiPt alloy as compared to Ni and Pd in NiPd alloy.

In figure 12 we display the frequency dependence of lattice thermal conductivity for $Ni_{50}Pt_{50}$ alloy at various temperatures, evaluated using the formulae given in equations (3) and (5). We note from figure 12 that as we increase the temperature the difference in lattice conductivity at a particular frequency is quite large in the lower temperature regime

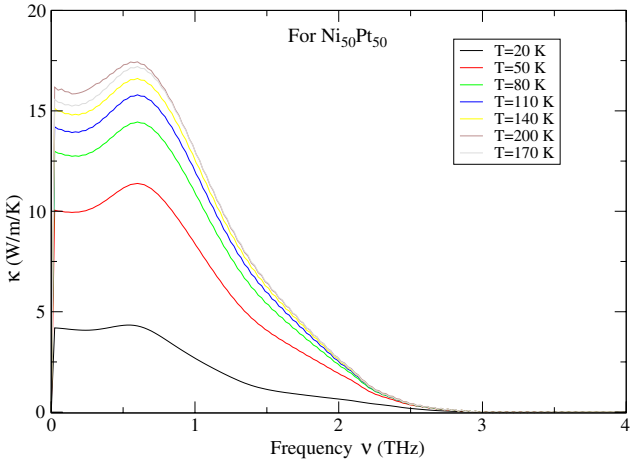

Figure 12. The configuration averaged lattice thermal conductivity versus phonon frequency ν (THz) at different temperatures T for $Ni_{50}Pt_{50}$ alloy.

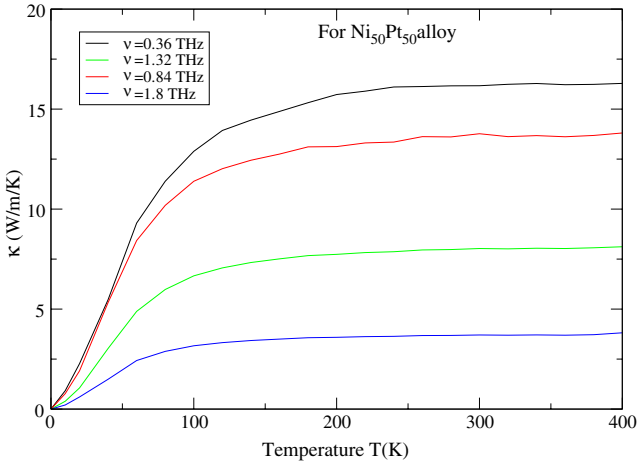

Figure 13. The averaged lattice thermal conductivity versus temperature T(K) at various cut-off frequencies ν_{cutoff} for $Ni_{50}Pt_{50}$ alloy.

(20 K $\leqslant T \leqslant$ 80 K); however, the difference starts to saturate as we go to higher temperatures. As discussed in the previous section, the extrapolated value of the $\kappa(\nu)$ curve from a value at $\nu > 0$ (next to $\nu = 0$) to a value at $\nu = 0$ is called the dc value of lattice thermal conductivity (κ_0). Figure 12 clearly shows that this dc value of the conductivity increases as we go on to increase the temperature. This is expected because in the dc limit the mechanism of heat conduction is transfer of energy between delocalized modes of equal energy by the heat current.

The behaviour of the $\kappa(\nu)$ versus ν curve in both NiPd and NiPt is qualitatively similar, but there are some quantitatively different features. The maximum in NiPt is located at a lower frequency as compared with NiPd. Also the overall magnitude of lattice conductivity in NiPd is higher than NiPt.

The temperature dependence of lattice conductivity for $Ni_{50}Pt_{50}$ alloy at various cut-off frequencies is shown in figure 13. The conductivity increases initially (in the low T regime) as

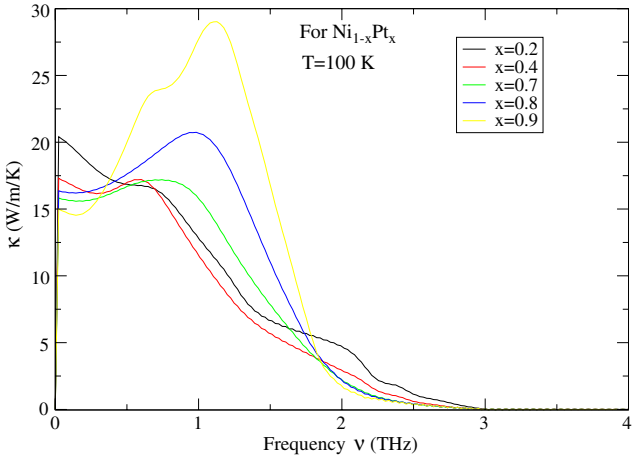

Figure 14. Frequency dependence of lattice thermal conductivity for various alloys $Ni_{1-x}Pt_x$ at $T = 100$ K.

an approximately quadratic function of temperature and ultimately increases smoothly to a T-independent saturated value. As far as such dependence of $\kappa(T)$ in the high temperature regime is concerned, the heat in this conduction channel is carried by non-propagating modes which are strongly influenced by the disorder but mostly not localized and therefore able to conduct by intrinsic harmonic diffusion. This is a smooth dependence which closely resembles the specific heat and saturates like the specific heat at high temperatures. Following Slack [3], we could call this part the '*minimum thermal conductivity*'. A number of authors have discussed that the low temperature dependence of $\kappa(T)$ shows a mild plateau-like region. In this regime the heat is mainly carried by the propagating long wavelength acoustic modes. The complex inelastic scattering processes then kill off the low frequency contribution at higher temperatures, leaving a peak which becomes the plateau. However, as in our calculation, the propagating modes may become reasonably well damped and are no longer able to carry much heat. In such cases the contribution of delocalized and poorly conducting vibrations takes over, giving a net result in good accord with Kittel's old idea. Under these circumstances the plateau-like region in the low temperature regime almost disappears. The damping of propagating modes is also amplified as we make the alloy more and more concentrated. This can easily be verified by looking at the results of reference [4], which shows that as we increase the concentration the plateau like region goes down and gets smoother.

In figure 14, we display the frequency dependence of lattice conductivity for NiPt alloys at various compositions, but at a fixed temperature $T = 100$ K. As before, each of the curves has a dip at the lowest frequency. It is important to notice that as we increase the Pt concentration x structure appears in the behaviour of $\kappa(\nu)$. This indicates that the structure arises due to the contribution of Pt atoms (with large mass) in the alloy.

The concentration dependence of lattice conductivity at a fixed phonon frequency $\nu = 1.05$ THz is plotted in figure 15. The various curves in this figure stand for various values of the temperature T starting from a lower value of 50 K to a higher value of 230 K. It is clear from the figure that the concentration dependence is almost symmetric about $x = 0.5$. It has been discussed by Flicker and Leath [13] within the framework of the coherent potential approximation that this asymmetry is a function of the size of the sample chosen, i.e. a large N leads to less asymmetry. They have verified this statement by performing two calculations,

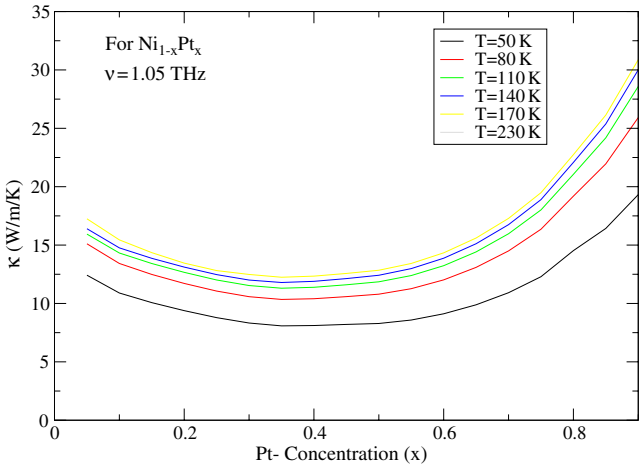

Figure 15. Lattice thermal conductivity versus Pt concentration for various temperatures T at phonon frequency $\nu = 1.05$ THz.

one for $N = 100$ and other for $N = 2000$. The concentration dependence in the latter case is more symmetric as compared to the former ones. In our case, the results shown in figure 15 are the optimal symmetric structure for the concentration dependence of κ. This is because our calculations are performed in the reciprocal space representation, which involves the entire lattice.

Figure 16 shows the frequency dependence of diffusivity $D(\nu)$ for various alloy compositions. The thick lines on the frequency axes show the extent of the frequency spectrum. These have been obtained from the density of states calculations presented in our first paper on the subject [15]. It is clear from figure 16 that there are basically two regions of large thermal diffusivity: one near the lower frequency region ($\simeq$0.5 THz) and the other around a somewhat higher frequency region ($\simeq$1.25 THz). But as we go on increasing the Pt concentration, the former region of large diffusivity starts decreasing gradually and becomes almost flat for the maximum Pt concentration of 90%. The latter region of large diffusivity sits on a portion of the frequency spectrum above the transverse acoustic vibrations. Here the modes have large velocities and are probably very effective carriers of heat. The approximate linear decrease in diffusivity starts at $\simeq$3 THz. But the location of the mobility edge in this case varies with composition in a slightly different way as compared to the case of the NiPd alloy. Figure 17 (bottom) shows the position of the mobility edge ν_c as a function of the alloy composition. As the concentration of heavy Pt increases, the band width of the frequency spectrum (which is proportional to the square root of the mass) shrinks and the position of the mobility edge within the band also shrinks. Figure 17 (top) shows the fraction of the frequency band which is extended. When the disorder is the strongest, i.e. at 50–50 composition, this fraction is a minimum.

One thing is very clear from the above discussion: that, in an alloy where mass disorder dominates and the force constant disorder is weak (as in the case of NiPd alloy), the complex disorder scattering processes try to localize more vibrational modes as compared to those in an alloy where both mass as well as the force constant disorder dominates (as in the case of NiPt alloy). The result can be interpreted in a slightly different way as *the role of force constant disorder in binary alloys is to make the vibrational eigenstates more delocalized*; i.e., the more dominant the force constant disorder is, the more delocalized the vibrational modes will be.

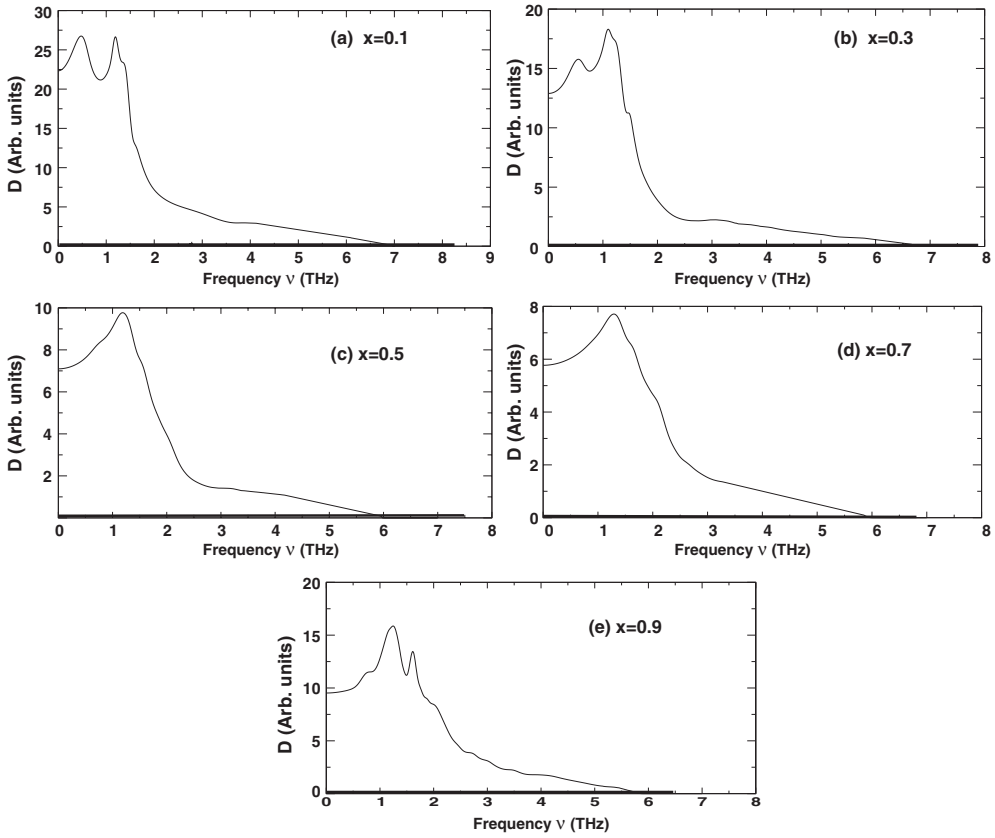

Figure 16. The configuration averaged thermal diffusivities $D(\nu)$ for $Ni_{1-x}Pt_x$ alloys. (a) $x = 0.1$; (b) $x = 0.3$; (c) $x = 0.5$; (d) $x = 0.7$; (e) $x = 0.9$. The broad line on the frequency axis shows the extent of the vibrational spectrum.

In figure 18, we present the concentration dependence of thermal diffusivity for various phonon frequencies ν. As in NiPd, the diffusivity is asymmetric about $x = 0.5$. However, this asymmetry reduces as we increase the phonon frequency. This asymmetry is also reflected in the behaviour of thermal conductivity with alloy composition.

4. Conclusions

We have performed a detailed numerical study of the theoretical formulation (AM) developed earlier by us for the lattice thermal conductivity of disordered binary alloys. We have demonstrated through our numerical results how this multiple scattering based formalism captures the effect of off-diagonal and environmental disorder present in the problem. The use of augmented space method to keep track of the configuration of the system and the block recursion method have made the implementation simple yet powerful. This is reflected in the satisfaction of the essential HSP analytic property of the diagonal green function in our earlier calculation [15]. A significant contribution of this article beyond the earlier theoretical approaches is the inclusion of force constant fluctuations properly in the theory. We have applied the formalism (AM) to two real disordered alloys, namely NiPd and NiPt. We have

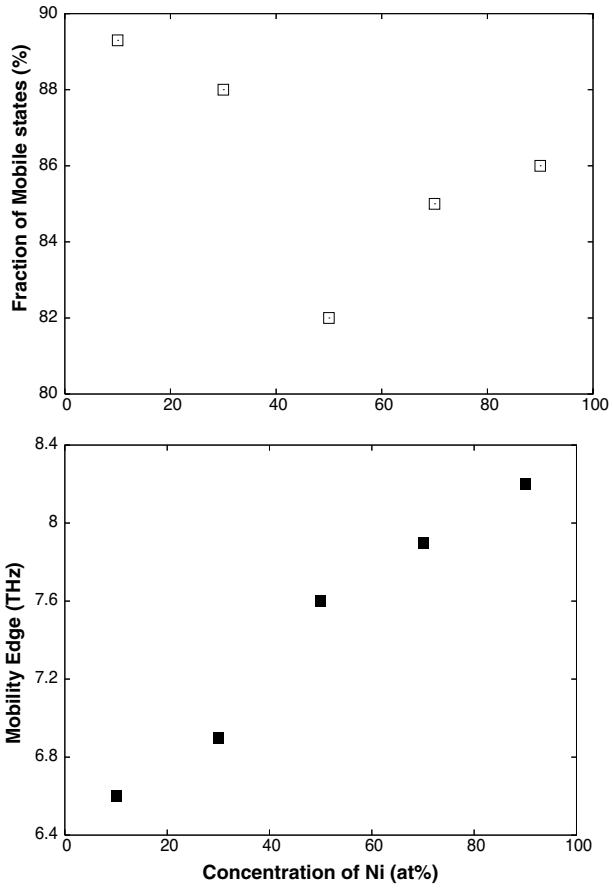

Figure 17. The position of the mobility edge (bottom) and the percentage of mobile phonon states (top) as a function of the alloy composition for NiPt alloy.

shown that the effect of disorder corrections to the current and the vertex correction on the overall shape of lattice thermal conductivity for both the alloys are very small. Comparatively, the effect is found to be more pronounced in NiPt alloy, which is due to the presence of strong disorder both in masses and force constants in this alloy. The prominence of the force constant disorder in NiPt alloy has also been demonstrated in the frequency dependence of lattice conductivity for various compositions of the $Ni_{1-x}Pt_x$ alloy. The saturation of lattice conductivity at higher temperatures has been shown for both the alloys. The concentration dependence of κ in $Ni_{1-x}Pd_x$ alloy has been shown to be more asymmetric about $x = 0.5$ than in $Ni_{1-x}Pt_x$ alloy. The numerical results on the harmonic diffusivity provide an interesting idea about the localization and delocalization of the vibrational eigenstates. It says that in disordered binary alloys 'the stronger the force constant disorder is, the more delocalized the vibrational modes will be'. This is why NiPt alloy has a larger fraction of delocalized states as compared to that in NiPd alloy. For both the alloys, however, we had no prior information about the species dependence of the force constants but rather choose a set of force constants intuitively as we have done earlier [8, 15]. A better understanding of the role of disorder in the transport properties of random alloys could be achieved with prior information about the force constants. These could be obtained from more microscopic theories, e.g. the first principles calculation on

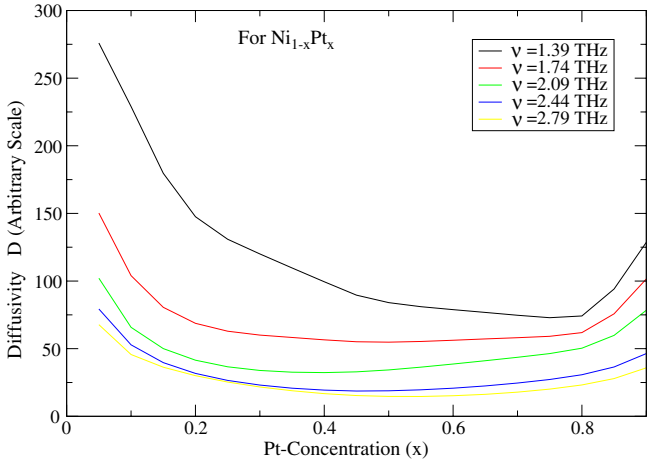

Figure 18. The averaged thermal diffusivity $D(\nu)$ versus Pt concentration at various cut-off frequencies ν_{cutoff} for $Ni_{1-x}Pt_x$ alloy.

a set of ordered alloys. Our future endeavour will be to rectify this and attempt to obtain the dynamical matrix itself from such microscopic theories.

Acknowledgments

One of the authors (AA) would like to thank the Council of Scientific and Industrial Research, Government of India, for a fellowship during the time when this work was carried out.

References

[1] Alam A and Mookerjee A 2005 *Phys. Rev.* B **72** 214207
[2] Kittel C 1948 *Phys. Rev.* **75** 972
Brich F and Clark H 1940 *Am. J. Sci.* **238** 613
[3] Slack G A 1979 *Solid State Physics* vol 34, ed H Ehrenreich, F Seitz and D Turnbull (New York: Academic) p 1
[4] Farrell T and Greig D 1969 *J. Phys. C: Solid State Phys.* **2** 1465
[5] Garber M, Scott B W and Blatt F J 1963 *Phys. Rev.* **130** 2188
Lindenfeld P and Pennebaker W B 1962 *Phys. Rev.* **127** 1881
[6] Bauer E, Gratz E, Hutflesz G and Muller H 1991 *J. Phys.: Condens. Matter* **3** 7641
[7] Srivastava B N, Chatterjee S, Sen S K and Chakraborty D K 1970 *J. Phys. C: Solid State Phys.* **2** S169
[8] Alam A and Mookerjee A 2005 *Phys. Rev.* B **71** 094210
[9] Klemes P G 1951 *Proc. R. Soc.* A **208** 108
Klemes P G 1960 *Phys. Rev.* **119** 507
[10] Ziman M J 1956 *Can. J. Phys.* **34** 1256
[11] Callaway J 1959 *Phys. Rev.* **113** 1046
[12] Parrot J E 1969 *J. Phys. C: Solid State Phys.* **2** 147
[13] Flicker J K and Leath P L 1973 *Phys. Rev.* B **7** 2296
[14] Ghosh S, Leath P L and Cohen M H 2002 *Phys. Rev.* B **66** 214206
[15] Alam A and Mookerjee A 2004 *Phys. Rev.* B **69** 024205
[16] Feldman J L, Kluge M D, Allen P B and Wooten F 1993 *Phys. Rev.* B **48** 12589